Second Harmonic Generation Imaging

Nirupama Bhattacharya, Eric Weiss

Physics 173 / BGGN 266

Spring 2012

1 Introduction

Second harmonic generation (or SHG) is a nonlinear optical process wherein a material interacts with intense laser light, resulting in the emission of light that is precisely doubled in frequency. Since different materials induce this effect to varying degrees, it can be used as an imaging technique, and as seen in recent literature, can be used in biological imaging as complementary to other nonlinear imaging modalities such as two photon microscopy.

2 Physics of SHG

Second harmonic generation involves the annihilation of two incident photons of frequency ω to form a new photon of frequency 2ω. Figure 1(right), shows an energy diagram of this process, which involves a virtual state that doesn't correspond to a real energy level of the molecule with which the photons are interacting. As a result, there is no true excited state; the quantum states of the molecules in the interaction volume don't change, for example, by electrons gaining energy and moving to different energy orbitals. This makes SHG distinct from other nonlinear optical processes that involve a true excitation (such as two photon excitation fluorescence) [6, 9].

2.1 Response of a Non-ideal Oscillator to Sinusoidal Forcing

It is possible to view the phenomenon as the response of a non-ideal oscillator to strong forcing. Inside of an optical medium, some of the electrons are susceptible to the influence of external electric fields; that is, an external field can induce a slight dipole moment by changing the charge distribution in a molecule. These dipoles can be viewed as small, nearly ideal harmonic oscillators which can radiate electromagnetic energy. Ideal damped harmonic oscillators (obeying the spring law $F = -kx$) respond to a sinusoidal forcing of frequency ω with oscillations of frequency ω. For general spring laws, however, the response will consist of a superposition of integer multiples of the driving frequency:

$$x(t) = Asin(\omega t) + Bsin(2\omega t) + Csin(3\omega t) + ... \tag{1}$$

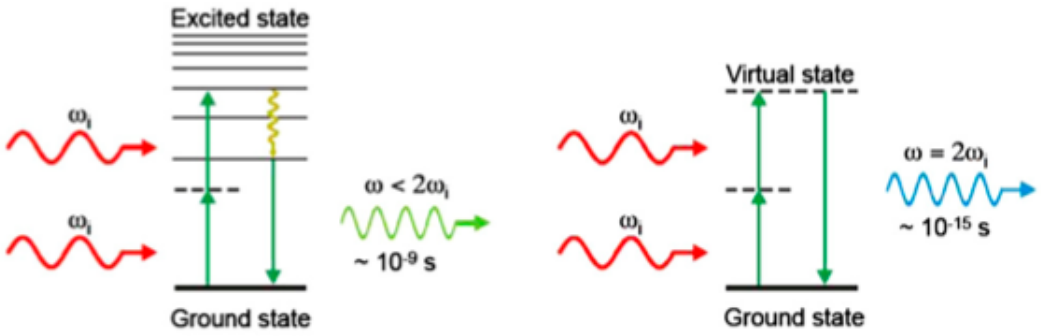

Figure 1: Jablonski diagram of two photon excitation emission (left), and second harmonic generation (right) [9].

Since the molecular dipole oscillators are nearly ideal, we can't normally detect the higher frequency terms because their coefficients are negligibly small. It is only by using light of extremely high intensity that we can begin to observe them.

2.2 Induced Polarization

Another way to understand the process of second harmonic generation is through the optical response of a material. In general, the optical response of a material can be expressed by the induced polarization $\vec{P}$

For a linear material

$$\vec{P} = \epsilon_0 \chi^{(1)} \vec{E} \tag{2}$$

where χ is the linear susceptibility, an indication of the degree of polarization of a material in response to an electric field. The higher the susceptibility, the greater the ability of the material to become polarized. $\vec{P}$ and $\vec{E}$ are the polarization and electric field vectors, respectively, and ϵ_0 is a constant.

In nonlinear optics, nonlinear effects appear as weak perturbations in addition to the linear expression given in (2). However, to observe these deviations from linear behavior, laser light with high enough power and intensity is required (see Section 4.1 for more about how this can be realized).

We can use a Taylor Series expansion of (2), and if we use component form, the expression is [5]

$$P_k = \epsilon_0 \left(\chi^{(1)}_{ik} E_i + \chi^{(2)}_{ijk} E_i E_j + \chi^{(3)}_{ijkl} E_i E_j E_l + ... \right) \tag{3}$$

The χ terms are susceptibility tensors, which can usually be reduced to coefficients if the SHG process is considered for a well defined direction. The linear χ term represents 1st order absorption and reflection. The 2nd order χ term represents second harmonic generation, sum and difference frequency generation. The 3rd order term represents multiphoton (such as two-photon) absorption, third harmonic generation, and anti-Stokes Raman scattering [2].

We can focus on the 2nd order term and expand it as follows:

$$\begin{aligned} P^{NL}_k &= \epsilon_0 \chi^{(2)}_{ijk} E_i E_j \; where \; E_i = \epsilon_i e^{-i\omega t} + \epsilon^*_i e^{i\omega t} \\ P^{NL}_k &= \epsilon_0 \chi^{(2)}_{ijk} \left(\epsilon_i \epsilon_j e^{-i2\omega t} + \epsilon^*_i \epsilon^*_j e^{i2\omega t} + \epsilon^*_i \epsilon_j + \epsilon_i \epsilon^*_j \right) \end{aligned} \tag{4}$$

From (4) we can see the frequency doubled terms as well as the DC electric field components.

Combining the interpretations in Sections 2.1 and 2.2, second harmonic generation can be described as a two step process:

1. The incident light with field E_1 excites a nonlinear polarization P, at frequency 2ω, where $P \propto E_1^2$
2. The induced polarization P radiates light with field E_2, at frequency 2ω

2.3 Noncentrosymmetry

Second harmonic generation has a noncentrosymmetry requirement: it only occurs in samples that do not have inversion symmetry. If we refer back again to (3) we can see why this must be true. A sample or interaction volume with inversion symmetry means our polarization and electric field vectors must be inverted: $\vec{E} \rightarrow -\vec{E}$, $\vec{P} \rightarrow -\vec{P}$. By inspection, this is only consistent with (3) if the even order terms are equal to zero, which means that no second harmonic generation can occur. This is why SHG imaging requires the use of noncentrosymmetric materials such as certain kinds of biomolecules, or inorganic crystals.

2.4 Forward Propagation

Light created through SHG propagates in the same direction as the light used to create it. By considering conservation of energy and momentum, and the fact that SHG is an energy-conserving process, we can see that this must be the case. Say we have two photons, each with frequency ω, energy E, and momentum $\vec{p}$, that are combined to create a new photon of frequency 2ω. This new photon has energy $E + E = 2E$ and momentum $\vec{p} + \vec{p} = 2\vec{p}$. Hence, the new photon propagates in the same direction as the original photons. If

we have a strongly converging laser beam, then two photons with somewhat different incident angles might combine to create a new photon with a new angle; however, the new photon will always propagate outward within the boundary of the cone defined by the incoming light, since the angle of the outgoing photon will be a weighted average of the angles of the incoming photons.

2.5 SHG vs. Two Photon Excitation-Emission

Although there are some similarities in the laser beam setups for both two photon and second harmonic generation microscopy, the fundamental physical processes behind these imaging modalities are distinct in the following ways:

- As explained in previous sections, there is no true excited state that occurs with second harmonic generation. With two photon absorption-emission however, we have fluorophores that are excited to an energized state and relax back to ground state by fluorescence [9].
- Because there is no true excited state that occurs with SHG, the process is very quick, and occurs on the order of femtoseconds. On the other hand, with two-photon fluorescence, the excitation emission interaction process takes nanoseconds to occur [9].
- As explained in the last section, because SHG is an energy conserving process and angular momentum is conserved, it must propagate in the forward direction only. With two-photon excitation-emission, there is some energy that is dissipated through relaxation of the excited state through several vibrational energy states (as shown in Fig. 1, left). As a result of this non conservation of energy and angular momentum, propagation occurs in all directions (2π solid angle).
- SHG is an intrinsic process- since there is no true excited state, there is no requirement of an external label. As a result, there should be no photobleaching or phototoxicity that occurs in the interaction volume. With two photon microscopy, fluorescent labeling is usually required, so although phototoxicity and photobleaching is alleviated in out-of-focus planes, these problems still occur in the focal plane [3].

3 Second Harmonic Generation Microscopy Applications

Second harmonic generation microscopy is gaining popularity for use with in-vivo imaging of noncentrosymmetric biological structures such as membranes and certain endogenous proteins that give a strong SHG signal. As a result of the physics described in Section 2, there are several advantages that SHG microscopy holds over similar imaging modalities.

Second harmonic generation involves minimal interaction with the sample, such that the biomolecules is unchanged in structure and energy configuration; the process is also energy conserving and preserves the coherence of the laser light.

Unlike fluorescence imaging modalities, when imaging endogenous proteins that give off an intrinsic SHG signal (such as collagen or tubulin), no staining or addition of fluorophore is required, and as a result, there are no adverse photobleaching or photoxicity effects that arise due to the creation of free radicals. SHG microscopy also retains the same intrinsic confocality (signal arises only from the focal plane) that two photon microscopy has, without any of the associated photobleaching problems. In combination with the use of infrared (IR) or near-IR incident laser light, deep sectioning of tissues is possible, which is advantageous when tissue samples are thick. This sectioning allows for 3D volume reconstruction by scanning the sample plane by plane and stacking these images together. Fig. 2 is an example of a 3D volume reconstruction of mouse muscle using SHG microscopy. Use of IR light also involves less scattering than visible light, which allows for improved resolution of the final image [1].

Some examples of widely used samples with SHG microscopy include collagen, myosin filaments, and microtubules. Due to the lack of center of symmetry of these molecules, an intrinsic SHG signal is emitted without the need of exogenous probes. The structure of collagen consists of three helical subdomains intertwined. Each individual helix is expected to produce an SHG signal, and by superposition, three produce an even larger signal. Since SHG imaging can reflect the structural content of these endogenous proteins in tissue samples, this imaging modality can be used to study pathology. For example, collagen structure and

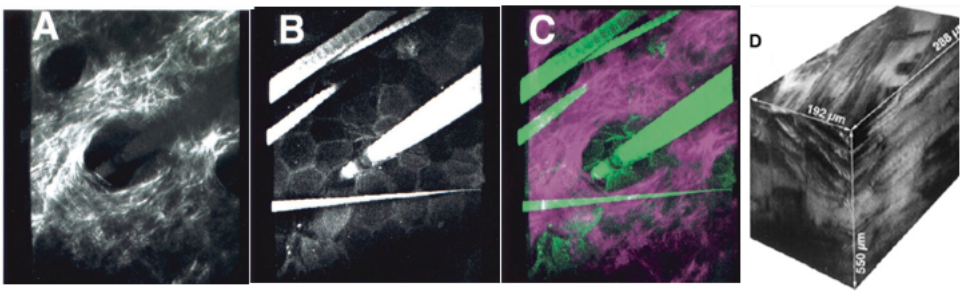

Figure 2: (A) SHG signal from the dermis layer of a mouse ear. (B) Two photon fluorescence signal from the same area. (C) False color spatially correlated overlay of both signals from (A) and (B). (D) 3D volume reconstruction of a sample of mouse lower leg muscle, optically sectioned using SHG microscopy, over a thickness of $550\mu m$ [1].

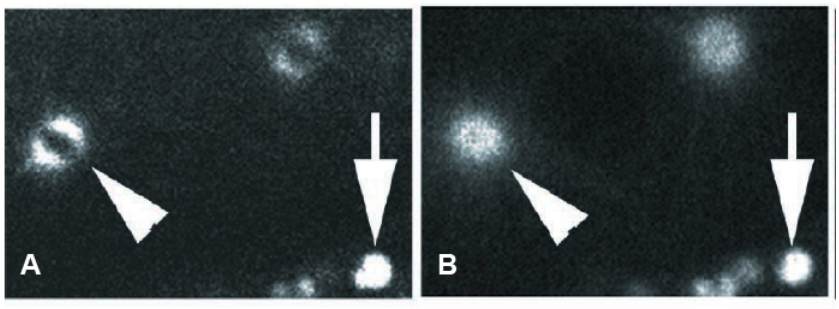

Figure 3: SHG (A) and two-photon fluorescence (B) signals of microtubules extending radially from spindle centers [1].

content differ between tumors and healthy tissue and SHG imaging can discriminate between the two types of tissue based on this fact. Since SHG is possible in vivo, it can also be used to assess tissue structure where the extracellular matrix is being remodeled, such as in wound healing and developing tissue [10].

SHG isn't the best modality to use for all types of molecules. For example, keratin is strongly auto fluorescent and gives a good two photon fluorescent signal, but no SHG signal. Collagen produces no two photon fluorescence signal, but is an efficient SHG source. For this reason, SHG microscopy is often combined with other modalities, most notably two photon, to simultaneously view parallel images. Both modalities are nonlinear and one can get these signals from the same focal plane, so the data obtained is complementary and can give a more complete picture of what is going on structurally in the sample. Figure 2A-C is a great example of this. Fig. 2A shows an SHG signal from the dermis layer of a mouse ear, which contains a lot of collagen. This figure doesn't show the hair follicle, however, since it contains keratin which doesn't give a SHG signal. Fig. 2B shows the two photon fluorescence image of the same area of the sample. Here we get a strong signal from the hair follicles. The most complete picture is obtained by combining both SHG and two photon signals (Fig. 2C) [1].

Fig. 3 shows SHG and two photon fluorescence images of microtubules extending radially away from the microtubule spindle and centrosomes. When using linearly polarized light, the SHG signal will change depending on how the polarization of the sample molecules aligns with the laser fundamental - the strongest signal arises from molecules whose dipoles are aligned with the laser polarization. This is why in Fig. 3A, we see a signal that is not circularly symmetrical - oppositely oriented SHG waves from oppositely oriented protein structures destructively interfere to create a lack of signal in the spindle mid-zone. So it's evident that important structural information is encoded in the SHG signal; however this can be misleading if we don't have a complementary imaging modality to compare with, such as the corresponding two photon fluorescent image in Fig. 3B. This example also demonstrates the potential for SHG polarization anisotropy to be used to determine the orientation of proteins and infer symmetry by rotating input laser polarization [1].

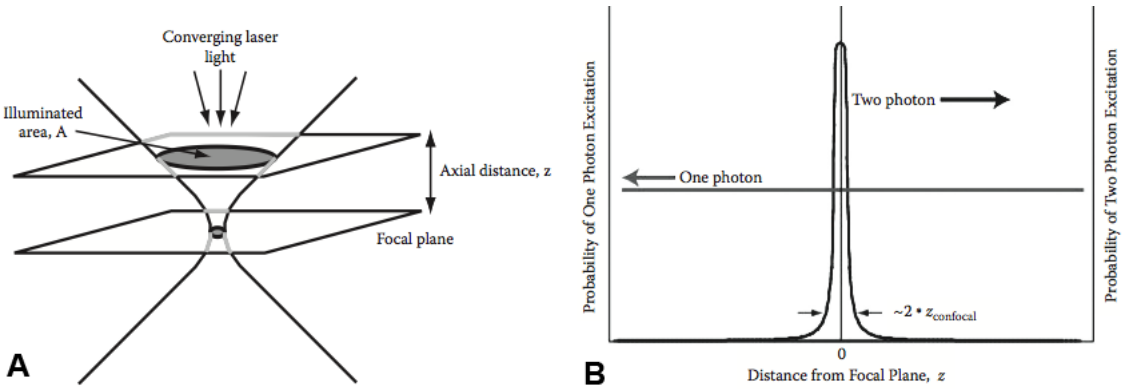

Figure 4: (A) Laser profile near the focal plane. (B) Probability of two photon excitation (or simultaneous interaction with sample in SHG), as a function of z [8].

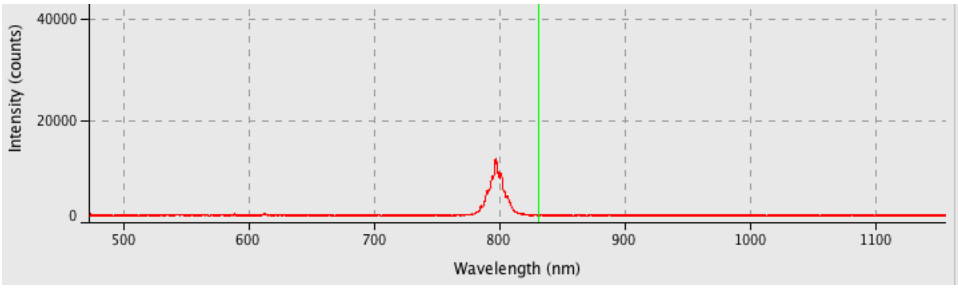

Figure 5: The Ti:Sapphire laser mode-locked to ∼800 nm, with a FWHM of ∼20 nm.

4 Experimental Setup

4.1 Lasers

As stated before, nonlinear interactions have a high probability of occurring when IR or near-IR light is concentrated in space and time [7].

High light intensity is produced by focusing a laser beam using an objective lens. The profile of a laser beam in the neighborhood of the focal plane, is shown in Fig. 4A. It is clear that the beam diameter is a function of z, such that the cross sectional area of the beam $A \propto z^2$. Since $I = \frac{Power}{A}, I \propto \frac{Power}{z^2}$ where z is the axial distance of a cross sectional beam slice, from the focal plane. We can see that intensity is highest at the focal plane, with a probability distribution given in Fig. 4B, showing that the probability of two photons interacting with the sample volume (either in an SHG process or two photon absorption) is nonzero only at or very close to the focal plane, and nowhere else [8].

High concentration in the time domain is generated by using ultrashort pulsed laser light, with pulses having high peak intensities. In this way we can have high temporally localized intensity but still maintain a low average power in order to avoid damaging the sample. This is particularly important when imaging biological tissue samples, since one of the main advantages that researchers strive for in using SHG microscopy over other modalities, is its limited invasiveness and alteration of the sample [8].

In our experimental setup we achieved high spatial and temporal light intensity by having a continuous wave laser sent into a mode-locking Ti:Sapphire IR laser that achieves the ultra short pulses by summing laser light of multiple frequencies so that destructive and constructive interference occur to create localized pulses in time (with pulse widths on the order of femtoseconds). In the spectral domain, this corresponds to a curve centered around a certain frequency, which is tunable. Fig. 5 shows our laser mode-locked at ∼800 nm with a FWHM of ∼ 20nm.

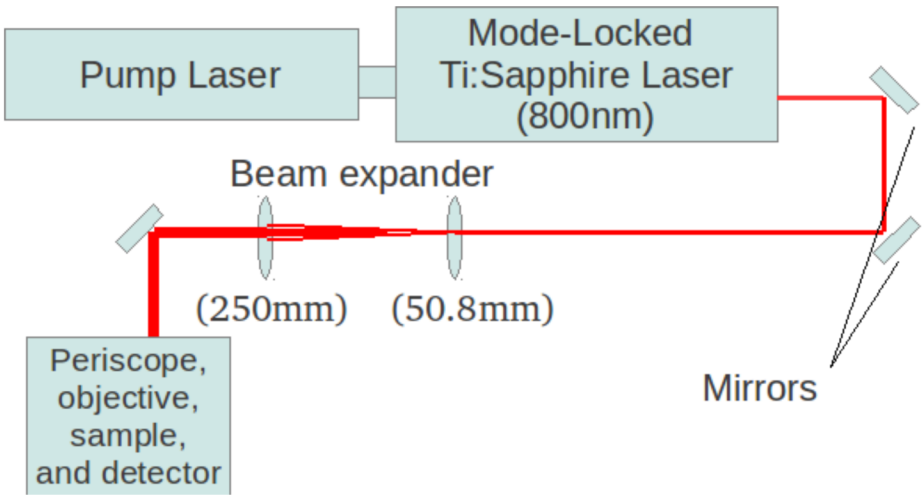

Figure 6: Our experimental setup for the laser beam path.

4.2 Beam Path

Our entire microscope setup was mounted on top of a vibration-isolated workbench. Our laser source consisted of the mode-locked Ti:Sapphire laser, pumped by a 5 Watt, 532 nm diode-pumped continuous-wave laser. The beam emitted from the Ti:Sapphire laser was approximately 1.5 mm in diameter. In order to create a beam wide enough to fill the back aperture of the 0.3 NA objective lens, we first directed it through a telescope expander consisting of two lenses (with focal lengths of 50.8 mm and 250 mm), which together created a telescope with expansion factor of ∼5. The widened (∼7.5 mm diameter) beam was then sent through a beam periscope, which directed it downwards into the objective lens. Fig. 6 shows a simplified diagram of our beam path.

4.3 Sample and Detector Assembly

Fig. 7A is a detailed diagram of our sample and detector assembly. The sample was held on a motorized stage with open-loop motors. Without access to a set of scanning mirrors, we controlled the X and Y motors by analog DC signals sent from Matlab through a National Instruments USB Data Acquisition (DAQ) unit. The signal from the DAQ had insufficient power to drive the motors, so we used a pair of high power op-amp circuits in voltage buffer configuration to supply the current needed to drive the motors.

A photomultiplier tube (PMT) along with a collector lens (focal length 12.77 mm) was mounted directly below the sample to detect the SHG light. In this configuration, the 400 nm SHG light as well as the 800 nm laser light and any light created through autofluorescence of the sample, will enter the photomultiplier tube. In order to prevent everything except the SHG light from making it to the PMT, we used three BG39 filters to block out the infrared laser light (transmission curve in Fig. 7B) and a bandpass filter (397-405 nm FWHM) to eliminate any light created through autofluorescence and only pass light that is exactly doubled in frequency (or halved in wavelength) compared to the incident IR light.

To minimize noise caused by external light sources, we enclosed the entire objective lens, sample stage, and detector assembly inside a cover of black foil (Fig. 8).

4.4 Stage Control and Data Acquisition Setup

Fig. 9 shows a basic overview of the input and output connections to the DAQ. We controlled the X and Y signals through separate output channels, and had the PMT signal connect to one input channel. In controlling the DAQ we found that there is often a latency period between when Matlab sends the output signal to the DAQ, and when the input channels actually start collecting data from the PMT; without knowing exactly what this latency period is, post-processing of the data becomes difficult since we don't know how signals coming from the PMT align with the movement of the stage. To solve this, we sent a copy

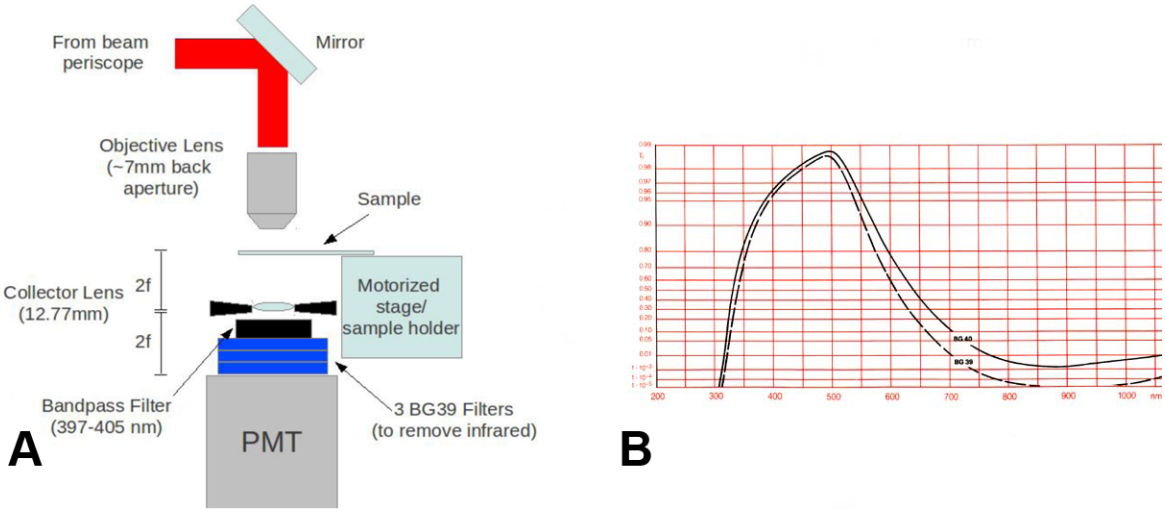

Figure 7: (A) Detailed diagram of our sample and detector assembly. (B) Transmission curve for the BG39 filter.

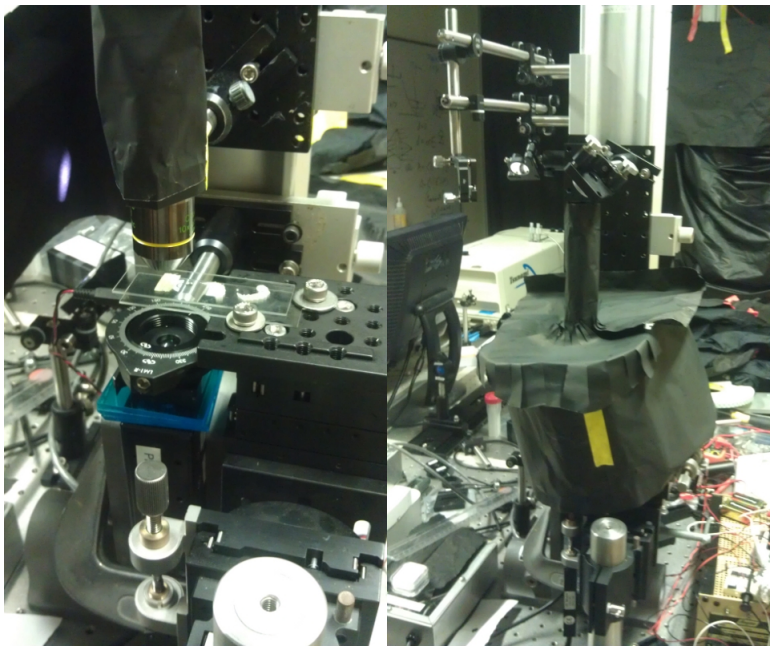

Figure 8: Our sample and detector assembly (left). Although normally the room lights were turned off, we added an extra shield over the assembly to protect from any stray light or reflections from monitors, etc... (right)

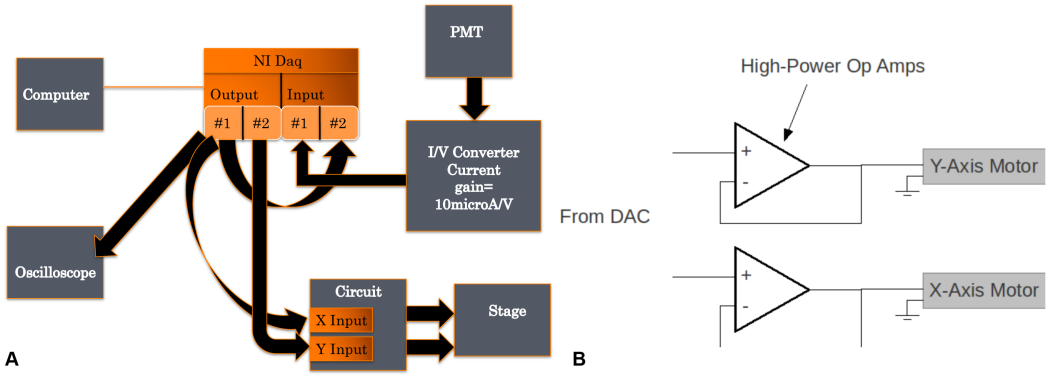

Figure 9: (A) Diagram of the input and output connection to our DAQ unit. (B) We added op-amps between the output of the DAQ and the motors in order to supply enough current to drive the motors.

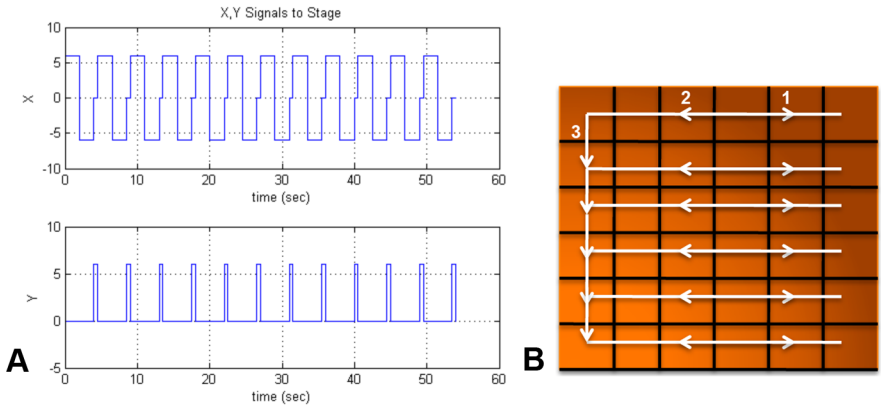

Figure 10: (A) The Matlab voltage signals that were sent to the DAQ and eventually to the X and Y motors. (B) The grid raster scan over the sample that corresponds to the set of signals given in (A).

of the X coordinate signal, into another input channel, so that during post processing, we could align the signals in time and correctly reconstruct our images.

As mentioned before, the current from our DAQ unit was not enough to drive the motors without adding a circuit consisting of high powered op-amps as a buffer in between the DAQ and the motors. Fig. 9 diagrams our DAQ connections and the op-amps included in the circuit.

Fig. 10 shows an example of X and Y coordinate signals that were sent to the stage, and the resulting raster scan pattern that resulted. We found that our motors had a "hysteresis" problem; that is, although the electronic signals sent to the motors were symmetrical across 0V (+/- voltages were equal so that the X coordinate motor should move forward the same amount it moved backward across each row scanned), in reality the motors actually moved more in one direction than the other, either due to friction, inertia, or some other effect that we were not able to correct for. As a result, our resulting images often were skewed due to this "drift" in the X coordinate range of the sample being scanned.

5 Results

5.1 SHG Crystal

The first samples we tried were mounted and unmounted barium borate birefringent inorganic crystals (BaB_2O_4 or BBO) which are common nonlinear optical materials. Both gave very strong second harmonic signals. Fig. 11A shows the unmounted crystal giving off blue-violet light. This is expected since our

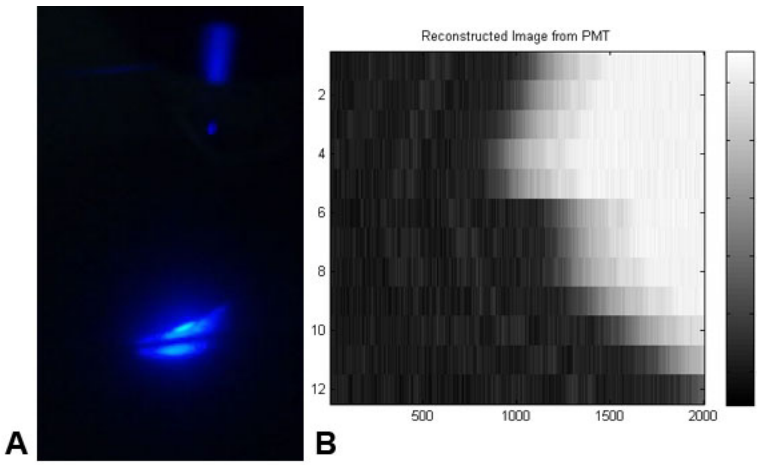

Figure 11: (A) The unmounted BBO crystal emitting second harmonic generated blue light. (B) Reconstructed image of the corner of the crystal that was scanned.

incident light from our mode-locked laser emitted 800 nm light and half this wavelength corresponds to the blue and violet light from the visible spectrum. To ensure that our emitted light was precisely half the wavelength of the incident light, we made use of the narrow bandpass filter described in Section 4.3. With a narrow transmission curve FWHM of 397-405 nm, this filter would block the second harmonic generated signal from the crystal if the mode-locking laser was tuned away from 800 nm. We experimented with this tuning and verified that a PMT only picked up a signal when the Ti:Sapphire laser was mode-locked to 800 nm, demonstrating that the second harmonic generated signal was indeed half the wavelength of the incident laser light.

Fig. 11B shows the final result of the post-processing that occurred in Matlab, in which we took the PMT signal in time and reconstructed the rows of the sample that were scanned. As is evident in the figure, we were able to successfully image the corner of our unmounted BBO crystal, although we can see some evidence of the drifting/hysteresis problem described in Section 4.4.

5.2 Biological Samples

We tried to image several biological samples to see if we could detect a second harmonic generated signal. We obtained two slide-mounted samples from David Matthews from the Kleinfeld Lab. The first was a thin slice of tissue of the area where a rat's whiskers emerge from the face - this sample was rich in collagen. The second sample was of a rat trigeminal nerve. The SHG signals from these samples was expected to be very weak compared to that emitted by the BBO crystals, but nevertheless, we believed the PMT to be sensitive enough to pick up changes in the SHG signal that reflected the tissue sample structure. Unfortunately, we were not able to detect any SHG signal emitted from these samples, even with completely dark surroundings (room lights off, light shield around the detector assembly and PMT, monitors covered, etc...)

Dr. Tsai referred us to [4], in which researchers were able to detect fairly strong SHG signals from plant polysaccharides. One of their samples was of celery petioles (part of the stalk) that contained collenchyma cells. We attempted to replicate their results by freehand slicing our own celery samples (both in the transverse plane and plane parallel to the stalk fibers), as shown in Fig. 12. Unfortunately, this didn't result in a detectable SHG signal either.

5.3 Future Directions

Currently, we are working to alter our experimental setup to try and detect SHG signals from the biological samples. In particular, we have swapped our 0.3 NA dry objective lens with a 0.8 NA oil-immersion lens, which would require the sample to be directly under and touching the objective lens. A higher NA objective

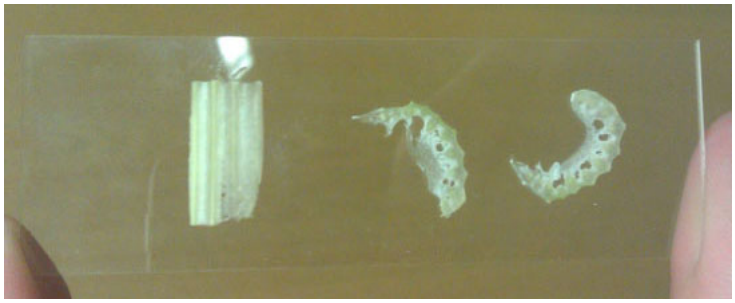

Figure 12: Celery petiole samples, sliced freehand.

means that more laser light will reach the sample, which should result in more SHG light being emitted from the sample.

On the collecting lens side of the assembly, we are experimenting with bringing the collecting lens and PMT closer to the sample stage. Since the PMT converts incident photons into an output that represents intensity of light for each point that is scanned across the sample, we are not trying to image the light from the sample onto the PMT detection area - that is, we don't need to focus the light near the PMT surface. All we need to do is make sure that the maximum amount of light being emitted from the sample plane, is captured by the PMT to increase the probability that it will detect a weak SHG signal. Therefore, we are planning to change our setup to include a larger collecting lens that is placed $\sim$1 focal length from the sample stage, with the PMT as close as possible underneath it. However, achieving this ideal setup is made difficult by that fact that we must keep our three BG39 filters that are used to block the IR laser light coming through the sample plane. This is a necessity since any laser light detected by the PMT is sure to drown out any weakly emitted SHG signal.

We might also consider whether the laser beam coming to the sample plane is fully optimized. Is the IR laser truly mode-locked, and is the sample plane truly at the exact z location where the maximum intensity of laser light occurs? Problems with any of these requirements could potentially be major reasons why the PMT is unable to detect SHG signals from the biological samples.

References

[1] Campagnola, P. "Three-Dimensional High-Resolution Second-Harmonic Generation Imaging of Endogenous Structural Proteins in Biological Tissues." Biophysical Journal 82.1 (2002): 493-508. Web.

[2] Campagnola, Paul J., and Leslie M. Loew. "Second-harmonic Imaging Microscopy for Visualizing Biomolecular Arrays in Cells, Tissues and Organisms." Nature Biotechnology 21.11 (2003): 1356-360. Web.

[3] Campagnola, Paul J., Heather A. Clark, William A. Mohler, Aaron Lewis, and Leslie M. Loew. "Second-harmonic Imaging Microscopy of Living Cells." Journal of Biomedical Optics 6.3 (2001): 277. Web.

[4] Cox, Guy, Nuno Moreno, and José Feijó. "Second-harmonic Imaging of Plant Polysaccharides." Journal of Biomedical Optics 10.2 (2005): 024013. Web.

[5] De Dood, Michiel, "Second-harmonic Generation." (2006).

[6] "Fundamentals and Applications in Multiphoton Excitation Microscopy." Nikon MicroscopyU. Nikon, Web. <http://www.microscopyu.com/articles/fluorescence/multiphoton/multiphotonintro.html>.

[7] Helmchen, Fritjof, and Winfried Denk. "Deep Tissue Two-photon Microscopy." Nature Methods 2.12 (2005): 932-40. Web.

[8] Tsai, P. & Kleinfeld, D. "In Vivo Two-Photon Laser Scanning Microscopy with Concurrent Plasma-Mediated Ablation: Principles and Hardware Realization." In Vivo Optical Imaging of Brain Function. Ed. Ron Frostig. Florida: CRC Press, 2009.

[9] Pantazis, P., J. Maloney, D. Wu, and S. E. Fraser. "Second Harmonic Generating (SHG) Nanoprobes for in Vivo Imaging." Proceedings of the National Academy of Sciences 107.33 (2010): 14535-4540. Web.

[10] Williams, Rebecca M., Warren R. Zipfel, and Watt W. Webb. "Interpreting Second-Harmonic Generation Images of Collagen I Fibrils." Biophysical Journal 88.2 (2005): 1377-386. Web.

[11] Zoumi, A. et al. "Imaging cells and extracellular matrix in vivo by using second-harmonic generation and two-photon excited fluorescence," PNAS, 99, 11014-11019 (2002)